Alternative phase diagram for the betaine phosphate-betaine arsenate mixed system

A. Almeida,[1,*] S. Sarmento,[2] M. R. Chaves,[1] J. L. Ribeiro,[3] L. G. Vieira,[3] M. L. Santos,[1] A. Klöpperpieper,[4] and A. M. Costa[1]

[1]*Departamento de Física da Faculdade de Ciências, IFIMUP, Universidade do Porto, Rua do Campo Alegre 687, 4169-007 Porto, Portugal*

[2]*IFIMUP, Universidade do Porto, Rua do Campo Alegre 687, 4169-007 Porto, Portugal*

[3]*Centro de Física, Universidade do Minho, Campus de Gualtar 4710-057 Braga, Portugal*

[4]*Fachbereich Physik, Universität des Saarlandes, 66200 Saarbrücken, Germany*

(Received 2 June 2006; published 25 August 2006)

The mixed solid solutions of ferroelectric betaine arsenate (BA) and antiferroelectric betaine phosphate (BP) are known examples of H-bonded materials with competing ferro and antiferro interactions. Dispersive anomalies detected in the dielectric loss at low temperatures have been tentatively associated with the stabilization of disordered phases such as re-entrant dipolarlike glassy phases. Despite extensive experimental studies of $(BP)_x(BA)_{1-x}$ mixed systems, the existence of such phases is doubtful so far. In an attempt to clarify the nature of the low temperature phase transition sequence of $(BP)_x(BA)_{1-x}$, we have undertaken detailed pyroelectric, dielectric, polarization reversal, Raman, and infrared studies as a function of temperature. In this work we shall present the experimental results for $x=0.25$ (BP25) and compare them with the ones previously reported for the two other intermediate compositions. We shall then propose a phase diagram alternative to the one already published for this system; moreover, we shall tentatively identify the possible underlying mechanisms, and discuss how such mechanisms evolve as a function of the BP concentration.

DOI: 10.1103/PhysRevB.74.064112 PACS number(s): 77.80.−e, 72.80.Ng, 63.20.−e, 78.30.−j

I. INTRODUCTION

Solid systems present many interesting types of phase transitions, such as those from a nonpolar high temperature state to a polar one at lower temperatures, with ferro, antiferro, or modulated long range order. Disordered cooperative systems have also attracted a lot of attention. These systems may arise whenever there is competition between different types of interactions, for example, in solid solutions of crystals where the pure compounds present different polar states at low temperatures.

Betaine arsenate (BA) and betaine phosphate (BP) are addition compounds of the amino acid betaine $[(CH_3)_3N^+CH_2COO^-]$ with arsenic and phosphoric acids, respectively.[1,2] Both BA and BP crystallize at room temperature in a monoclinic structure, belonging to the space groups $P12_1/n1$ and $P12_1/c1$, respectively. Their microscopic structures are built from parallel quasi-one-dimensional chains, where each single chain is formed by arsenate or phosphoric tetrahedra linked through strong hydrogen bonds.[3,4] One betaine molecule is attached to each tetrahedron by two weaker hydrogen bonds. The polar axis is parallel to the chain direction in both compounds, but while in BA lies on the glide plane n, in BP coincides with the helicoidal axis 2_1.

Above room temperature both compounds exhibit one structural phase transition from a prototype high temperature phase to a ferroelastic (betaine arsenate; $T_{c1}=411$ K) or an antiferrodistortive (betaine phosphate; $T_{c1}=365$ K) phase.[4–6] In both cases, the phase transition is accompanied by an inclination of the tetrahedron and the betaine groups relatively to the chain, but while in BA the inclination has the same direction for two neighbor single chains, in BP an opposite rotation is preferred.[3,4]

At lower temperatures both compounds undergo further structural transitions.[1,2,6] Owing to different configurations, interchain and intrachain competitive interactions lead to the stabilization of a ferroelectric dipolar order in the case of BA ($T_{c2}=119$ K), whereas in BP an antiferroelectric order is favored ($T_{c2}=86$ K).[1,5,6] The ferroelectric (antiferroelectric) state arises from the parallel (antiparallel) arrangement of neighbor ferroelectrically ordered single chains.[4,6,7]

The effect of deuteration on the low temperature transitions indicates that these are very likely triggered by the ordering of two independent protons within each single chain.[5,7,8] However, other molecular motions may as well contribute to the structural instabilities[4–6,8,9] and the mechanism of the transitions may be rather complex due to the coupling between the molecular lattice and the protons in the hydrogen bonded chains.

Mixed crystalline solutions of the two compounds $(BP)_x(BA)_{1-x}$ can be formed in the range $0<x<1$. A previous experimental characterization of the solid solution[7] indicated that a long range ferro or antiferro order prevailed throughout the whole concentration range, at least for temperatures above 40–50 K. At lower temperatures, some dispersive anomalies in the dielectric loss have been interpreted as evidence for the stabilization of reentrant dipolar glass phases, with Vögel-Fulcher (G_1) or Arrhenius (G_2) kinetics.[7,10] However, these conjectured low temperature glassy phases seemed to be curiously stable against applied bias fields because the temperatures of the dispersive anomalies in the dielectric loss were nearly field independent.[11] On another hand, their existence could not be corroborated so far, either by x-ray[6] or by pyroelectric measurements over repeated thermal cycles.[12] Hence, the low temperature microscopic structure and dipolar ordering of the $(BP)_x(BA)_{1-x}$ mixed system remains unclear.

In an attempt to further understand these issues, we have undertaken detailed pyroelectric, dielectric, and polarization

reversal studies of the $(BP)_x(BA)_{1-x}$ mixed system, complemented with Raman and infrared spectroscopic investigations. The results obtained for the compositions $x=0.75$ (BP75) and $x=0.52$ (BP52) were previously reported.[12,13] In the present work, we shall present the results obtained for $x=0.25$ (BP25) and compare them with those obtained for the other compositions. This comparative investigation of the temperature and composition dependence of the properties of the mixed system will allow us to propose a phase diagram, alternative to the one previously presented.[7]

II. EXPERIMENTAL

The $(BP)_x(BA)_{1-x}$ complex was prepared in an aqueous solution by mixing betaine, arsenic, and phosphoric acids in an appropriate ratio. Single crystals were grown from a saturated aqueous solution by slow evaporation at ambient temperature.

Single crystal rectangular parallelepiped-shaped samples were prepared for dielectric, Raman, and infrared reflectivity measurements. The edges of optically polished parallelepipeds for spectroscopic studies were chosen as follows: $X \| a$, $Y \| b$, and $Z \| c^*$.

The low frequency complex dielectric constant was measured along the **b** direction in $(BP)_x(BA)_{1-x}$ $(x>0.15)$,[14] with an impedance analyzer, under an ac electric field of 1 V cm^{-1}. The polarization reversal was studied at different fixed temperatures with a modified Sawyer-Tower circuit, driven at the frequency of 0.5 Hz. The electric current was measured by heating and cooling the samples at the rate of $\approx$1 K min^{-1}, with a standard short circuit method[15] in sequential thermal cycles: first, a zero-field cooling run (ZFC)—with no applied bias electric field—then a field heating (FH) and a field cooling (FC) run—with an applied dc electric field—and finally, a zero-field heating run (ZFH), with no applied electric field. The polarizations were calculated by time integration of the pyroelectric currents. Sample temperature was measured with accuracy better than 0.1 K.

Raman spectra were recorded in the spectral range of 6–3500 cm^{-1}, using a coherent INNOVA 90 polarized argon laser operating at $\lambda=514.5$ nm in a right-angle geometry. The scattered radiation was analyzed using a Jobin-Yvon T64000 spectrometer equipped with a charged-coupling device and a photon-counting detector. The spectral slit width was about 1.5 cm^{-1} wide. The spectra were registered in the temperature range 12–300 K at constant temperature after a waiting time of about 15 min. The frequency, width, and intensity of Raman modes were determined by fitting a model of independent damped harmonic oscillators to the experimental data.[12]

The infrared reflectivity measurements were performed in the spectral range 40–4000 cm^{-1} with a Bruker IFS 66V FTIR spectrometer. The spectra were obtained in a quasinormal incidence using a combination of sources (Hg arc and globar lamps), detectors (DGTS with KBr or polyethylene windows), and beam splitters (KBr and Mylar of several thicknesses). An aluminum mirror was used as reference. The resolution was better than 2 or 4 cm^{-1}, respectively, for the 20–400 cm^{-1} and 400–4000 cm^{-1} spectral range. The spectra were registered at a constant temperature after a waiting time of about 20 min to achieve a good thermal equilibrium. The complex dielectric function along the monoclinic b axis $\varepsilon_b=\varepsilon_b'+i\varepsilon_b''$ was calculated from the polarized infrared reflectivity $(\vec{E} \| \vec{b})$ spectra via the Kramers-Krönig inversion. The values of the frequencies of transverse $(\Omega_{TO})$and longitudinal (Ω_{LO}) optical modes were then evaluated from the location of the maxima of $\varepsilon_b''(\omega)$ and $\mathrm{Im}(1/\varepsilon_b)=\varepsilon''/\varepsilon'^2+\varepsilon''^2$, respectively. This evaluation allowed us to estimate the value of the dielectric strength of the ith mode $(\Delta\varepsilon_i)$ via

$$\Delta\varepsilon_i = \frac{\varepsilon_\infty}{\Omega_{TO,i}^2} \frac{\prod_k (\Omega_{LO,k}^2 - \Omega_{TO,i}^2)}{\prod_{k\neq i} (\Omega_{TO,k}^2 - \Omega_{TO,i}^2)};$$

ε_∞ was obtained from the asymptotic value of the reflectivity (frequencies above 4000 cm^{-1}).

III. EXPERIMENTAL RESULTS

A. Dielectric constant

Figure 1(a) shows the real part of the dielectric constant versus temperature, $[\varepsilon'(T)]$, for BP25: the solid line corresponds to the data measured at 10 kHz with an impedance analyzer, and the circles represent the values of ε' obtained from linear fits of the low field region of the $P(E)$ curves, which were obtained at 0.5 Hz. For BP25, there is a remarkable agreement between these two sets of results obtained at very different frequencies, which shows that there is no low frequency dielectric dispersion (<10 kHz). The imaginary part of the dielectric constant versus temperature, $[\varepsilon''(T)]$, measured at 100 kHz, is also presented in the inset. The corresponding data obtained for BP52 (Ref. 13) and BP75 (Ref. 12) is shown in Figs. 1(b) and 1(c), respectively, for comparison. The arrows indicate phase transition temperatures. It is interesting that the values of $\varepsilon'(T)$ obtained at 10 kHz and 0.5 Hz do not agree as well for BP52 and BP75, at low temperatures, as they do for BP25.

As seen in Fig. 1(a), $\varepsilon'(T)$ measured on BP25 presents a maximum at $T_{c2,a}\approx 96$ K. At a very low frequency range [see data obtained from the $P(E)$ curves], $\varepsilon'(T)$ also displays a small shoulder at $T_{c2,b}\approx 74$ K, while $\varepsilon''(T)$ discloses an additional small maximum at $T_{c3}\approx 35$ K. These three dielectric anomalies delimit four temperature ranges where different polar properties may occur. The $\varepsilon'(T)$ and $\varepsilon''(T)$ curves obtained for BP25 are qualitatively similar to those of BP52 [see Fig. 1(b): $T_{c2,a}\approx 85$ K, $T_{c2,b}\approx 75$ K, and $T_{c3}\approx 30$ K), but differ from those of BP75 [see Fig. 1(c): $T_{c2}\approx 85$ K and $T_{c3}\approx 52$ K].

B. Polarization reversal curves

Figure 2 shows typical examples of polarization vs applied ac electric field $[P(E)]$ curves for BP25 [Fig. 2(a)], along with those observed for BP52 [Fig. 2(b)] and BP75 [Fig. 2(c)].[12,13] The data were taken at different fixed temperatures with a measuring ac electric field driven at a frequency of 0.5 Hz. The $P(E)$ curves observed in the case of

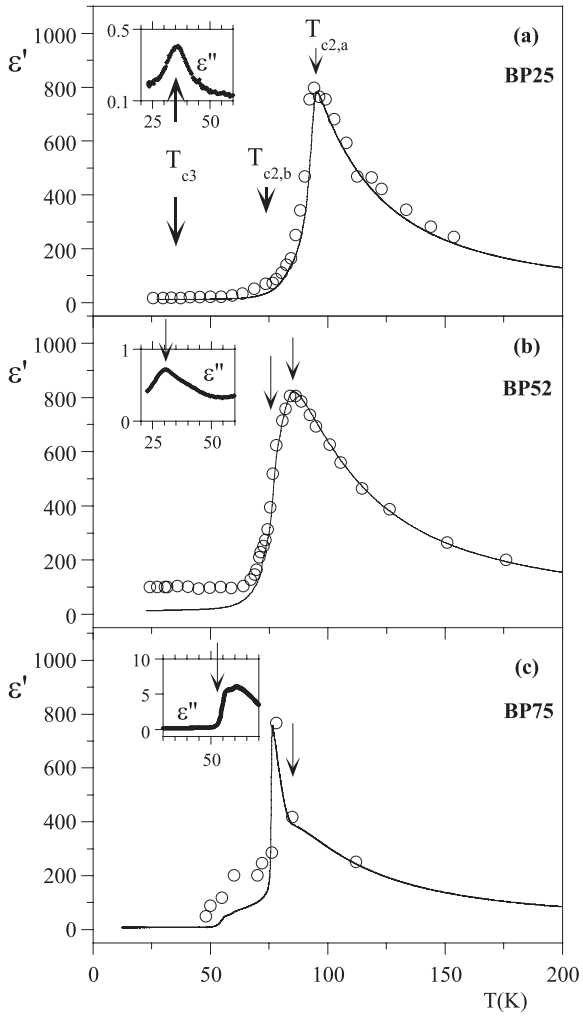

FIG. 1. Real part of the dielectric constant $\varepsilon'(T)$ obtained for BP25 (a), and corresponding results previously reported for BP52 (b) (Ref. 13); and BP75 (c) (Ref. 12). The solid line represents $\varepsilon'(T)$ measured with an impedance analyzer, while the circles correspond to $\varepsilon'(T)$ obtained from the slope of linear fittings to the central part of polarization vs applied electric field $[P(E)]$ curves at 0.5 Hz. The insets show $\varepsilon''(T)$. Phase transition temperatures are indicated by arrows.

BP25 [Fig. 2(a)] are complex and present a certain similarity with those observed in BP52 [Fig. 2(b)]. In Fig. 3 we compare the temperature dependence of the sublattice polarization [Fig. 3(a)], coercive electric field [Fig. 3(b)], critical field [Fig. 3(c)] and internal bias field [Fig. 3(d)], observed in the three compositions investigated.

The $P(E)$ curves obtained for BP25 [Fig. 2(a)] reveal a paraelectric behavior above $T_{c2,a} \approx 96$ K and an antiferroelectric response between $T_{c2,b} \approx 74$ K and $T_{c3} \approx 35$ K. The double hysteresis loops observed for BP25 are noncentered and highly asymmetric, revealing the presence of a very strong internal bias electric field (≈ 2.6 kV/cm at $\approx T_{c2,b}$). Moreover, the saturated right half of the loops appears elongated and ends in a straight line with a slope unexpectedly higher than that observed at zero fields, which is linearly related to the low frequency dielectric constant. Between $T_{c2,b} \approx 74$ K and $T_{c3} \approx 35$ K, we observe that, as the temperature decreases, the saturated right half of the hysteresis loops becomes larger while the unsaturated left half shrinks. This effect is most directly related to the increase of the internal bias field as the temperature decreases [Fig. 3(d)].

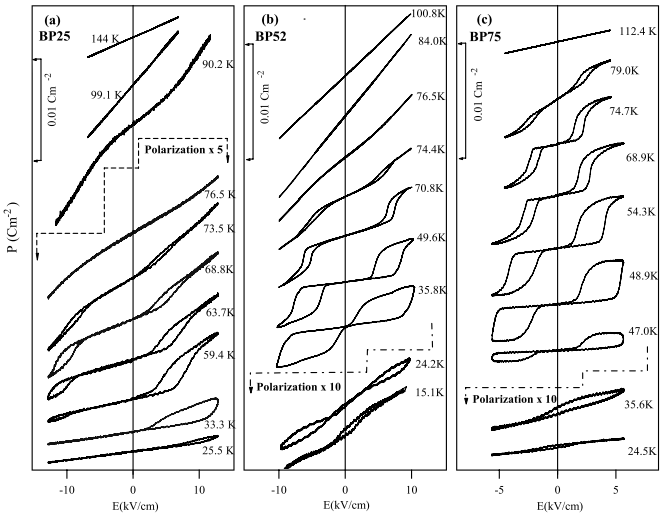

FIG. 2. Polarization as a function of an ac applied electric field operating at a frequency of 0.5 Hz, obtained for BP25 (a), BP52 (b), and BP75 (c), at different fixed temperatures. The phase transition temperatures are as follows: $T_{c2,a} \approx 96$ K, $T_{c2,b} \approx 74$ K, $T_{c3} \approx 35$ K for BP25; $T_{c2,a} \approx 85$ K, $T_{c2,b} \approx 75$ K, $T_{c3} \approx 30$ K for BP52; $T_{c2} \approx 85$ K, $T_{c3} \approx 52$ K for BP75.

As shown in Fig. 2(b), BP52 also presents a paraelectric behavior above $T_{c2,a} \approx 85$ K and an antiferroelectric response between $T_{c2,b} \approx 75$ K and $T_{c3} \approx 30$ K, with a sublattice polarization that is much larger than in the case of BP25. The double hysteresis loops are nearly symmetrical but slightly noncentered, which indicates the presence of an internal electric field (≈ 700 V/cm), although much smaller than the one observed in BP25. The value of this field decreases very slightly on cooling [Fig. 3(d)].

Between the temperature $T_{c2,a}$, where the maximum value of ε' [maximum slope of the $P(E)$ curve at zero ac electric field] is attained, and at the onset of antiferroelectric loops, at $T_{c2,b}$, we observe nonlinear and complex shaped $P(E)$ curves both in BP25 and BP52 (see Fig. 2). This behavior is much more evident and occurs over a larger temperature range in the case of BP25 [Fig. 2(a)], but is still clear in BP52 [see in Fig. 2(b) the curve taken at 76.5 K as one example]. On the other hand, in the case of BP75 we find no such behavior[12] [see Fig. 2(c)]. Note in Fig. 2(a) that, in BP25, the shape of some of the antiferroelectric loops observed below $T_{c2,b}$ still resembles the nonlinear $P(E)$ curves observed in the range $T_{c2,a} > T > T_{c2,b}$, because of the high slope observed in the saturated part of the curves. This feature is well illustrated in the loops depicted in Fig. 2(a) taken at 63.7, 68.8, and especially at 73.5 K.

Below $T_{c2,b} \approx 74$ K, the coercive field of the double hysteresis loops observed in BP25 continuously increases as the temperature decreases down to $T_{c3} \approx 35$ K. Below this temperature, both the coercive field and the sublattice polarization decrease sharply and the double loops disappear [see Fig. 2(a)]. This vanishing of the antiferroelectric loops can-

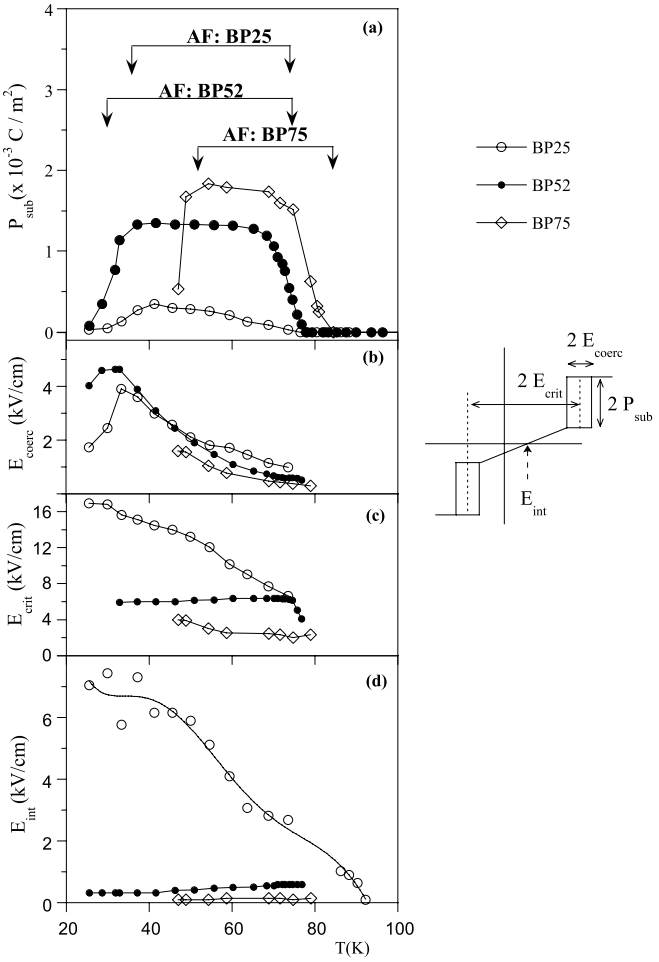

FIG. 3. A comparison of the sublattice polarization (a), coercive field (b), critical field (c), and internal field (d), as a function of temperature, for the three compositions studied. By comparison, note that the sublattice polarization of the pure BP is $\sim 4 \times 10^{-3}$ cm^{-2} (Ref. 2). The large asymmetry in the $P(E)$ curves of BP25 caused by the strong internal field allowed a reliable estimate of the critical field up to values of 16 kV/cm, even though we were experimentally limited to ±13 kV/cm.

not be related to a sudden increase of the internal or critical fields, as can be clearly concluded from Figs. 3(b)–3(d). Moreover, the temperature of this change coincides with T_{c3}, a temperature at which $\varepsilon''(T)$ shows a maximum (see Fig. 1).

A similar behavior has been observed in the case of BP52. The comparison of Figs. 1(b), 2(b), and 3(a) shows that the maximum of $\varepsilon''(T)$ that occurs at $T_{c3} \approx 30$ K in this composition also coincides with the rapid decrease in the sublattice polarization, which changes from its saturation value to zero over a temperature interval of ≈10 K.[13] Here also, the antiferroelectric loops vanish and only an incipient ferroelectriclike response is observed at low temperatures. Also, in the case of BP75, a steep decrease of the sublattice polarization is observed at $T_{c3} \approx 52$ K [Fig. 2(c)], a temperature at which $\varepsilon''(T)$ shows a discontinuous decrease [see Fig. 1(c)].[12]

The temperature dependence of the sublattice polarizations measured in the three compositions allows us to delimit, in each case, the temperature range of stability of the

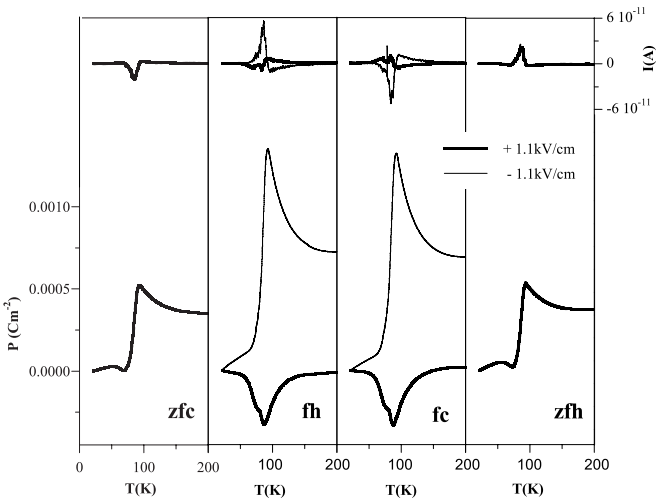

FIG. 4. Pyroelectric current (above) and polarization difference calculated by time integration of the pyroelectric current (below) obtained for BP25 on two zfc-fh-fc-zfh thermal cycles with bias field of opposite sign ($E_{\text{bias.}} = \pm 1.1$ kV/cm).

antiferroelectric phase. Furthermore, while the temperature dependence of the coercive electric field is qualitatively similar for the three compounds studied, the temperature dependence of the internal and critical field for BP25 is clearly different from those in BP52 and BP75 [Figs. 3(c) and 3(d)]. Whereas for these two compositions, $E_{\text{int}}(T)$ and $E_{\text{crit}}(T)$ are basically temperature independent, in BP25 both of the fields increase monotonically as the temperature decreases.

C. Pyroelectric effect and thermal cycles

The results obtained for BP25 from pyroelectric measurements performed in the sequential thermal cycles previously described are summarized in Fig. 4. As shown in Figs. 4(a) and 4(d), time integration of the pyroelectric currents obtained without an applied electric field (zfc and zfh, respectively), gives rise to polarization curves that reproduce remarkably well the shape of $\varepsilon'(T)$, presented in Fig. 1. Since the material does not present a ferroelectric polarization (reversible under external field), this proportionality between polarization and susceptibility indicates the existence of an internal field that exists already within the paraelectric phase. From the values of the dielectric constant and electric polarization obtained above $T_{c2,a}$, we could estimate a value of the order of 350 V/cm for the internal field in this temperature range. Below $T_{c2,a}$, the internal field could not be determined from pyroelectric data owing to the complex polar processes contributing to the current. However, as it has been referred to above, the existence of such an internal field is clearly demonstrated from the $P(E)$ curves obtained below $T_{c2,b}$ [see, e.g., Fig. 2(a)].

Figures 4(c) and 4(d) correspond to data measured under applied electric fields of ±1.1 kV/cm, on heating (fh) and cooling runs (fc), respectively. The polarization curves obtained from the time integration of the pyroelectric current measured under fields of opposite signs present different maximum values and shapes. When the external electric field

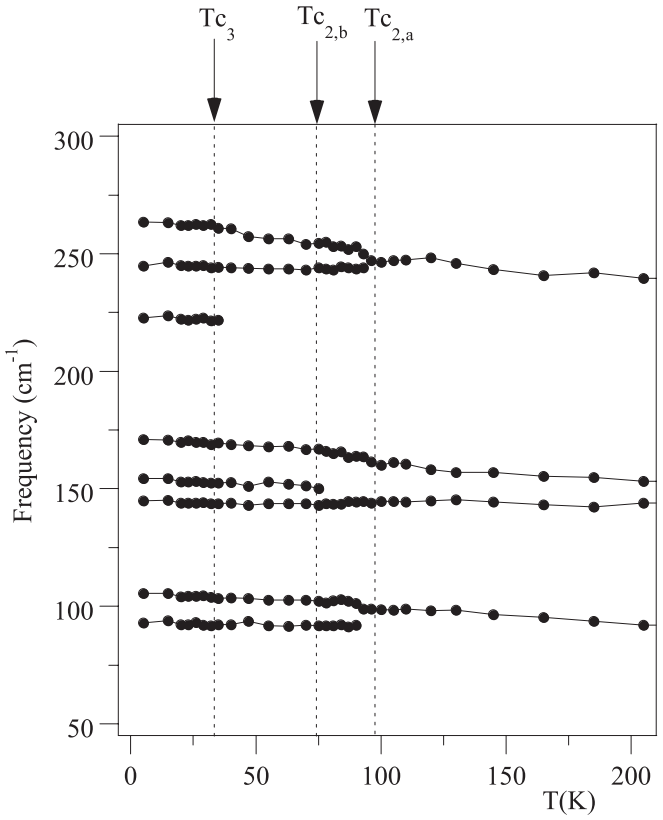

FIG. 5. Temperature dependence of the frequency of the modes fitted to the Raman spectra of BP25 obtained in $x(YY)z$ geometry.

applied is positive, the $P(T)$ curve develops a shoulder on the lower temperature side of the maximum. It is interesting to note that a similar shoulder in $\varepsilon'(T)$ curves was previously observed under high hydrostatic pressure, for several different concentrations of BP.[7]

The results presented in Fig. 4 give no evidence for ergodicity breaking. In fact, the values of the polarization appear to depend only on intensive variables such as temperature and electric field, and not on the past history of the sample. A similar apparently ergodic behavior was found for BP75.[12] Only in the case of BP52 was it possible to find some evidence for a nonergodic behavior below $T^* \approx 70$ K,[13] a surprisingly high temperature that is still well within the range of the antiferroelectric phase.

D. Raman and infrared spectroscopies

Figure 5 shows the temperature dependence of the frequency of external modes in BP25, for the $x(YY)z$ geometry. As can be seen, each of the bands located at about 90 and 240 cm^{-1} (at $T=200$ K) split into two bands near $T_{c2,a}$. Also at T_{c3}, one observes the activation of a band at about 225 cm^{-1}. Moreover, the band located near 150 cm^{-1} at $T=200$ K, ascribed to the out of plane bending of the betaine and the tetrahedral groups,[16–19] also splits into two bands near $T_{c2,b}$. These results indicate that at least local symmetry breakings occur at the phase transition temperatures $T_{c2,a}$, $T_{c2,b}$, and T_{c3}, clearly detected by dielectric, pyroelectric and polarization reversal measurements.

Let us consider now one selected example shown among the internal modes. A characteristic which is often considered distinctive for pure BP and BA is the appearance, at low temperature, of double Raman lines for BP in the case of the betaine internal modes around 2997 cm^{-1} (antisymmetric stretching CH modes),[8] where only one Raman line is observed for BA throughout the whole temperature range. The different behavior of the antisymmetric stretching CH modes in BP and BA is most likely related to the different geometrical configuration of the betaine molecules in the two compounds.

Since in the mixed compounds $(BP)_x(BA)_{1-x}$ for $x>0.15$ the geometrical configuration of the betaine molecules is the same as that of the pure BP,[14] we have followed Freitag *et al.*[8] in fitting the Raman spectra of BP25, BP52, and BP75 always with two modes, throughout the whole temperature range.

The results are presented in Fig. 6. The difference in the frequencies of the two fitted modes, $\Delta\nu$, is also presented in Fig. 6 as a function of temperature, for BP25, BP52, and BP75.[12,13] For both BP52 and BP75, there is a marked increase in $\Delta\nu(T)$ below $T_{c2,a}$ and T_{c2}, respectively. BP75 presents a jump in $\Delta\nu$ at T_{c3}, which is not observed in BP52. The behavior of $\Delta\nu$ observed in BP25 is markedly different from that observed in the other two compositions: it shows a tiny peak at $T_{c2,a}$ and only hints of the phase transitions at $T_{c2,b}$ and T_{c3}.

The infrared (IR) and Raman spectra often give complementary information, which is why it is interesting to have results from both spectroscopies. Figure 7 shows the dispersion of the imaginary part of the dielectric function ε''_b, ob-

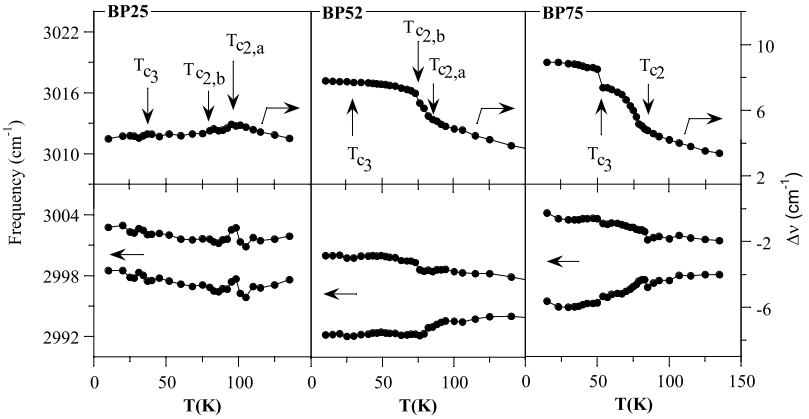

FIG. 6. The internal betaine modes around 2997 cm^{-1} (CH modes) fitted with two peaks in the whole temperature range for the three compositions studied. The frequencies obtained are presented here as a function of temperature (lower portion of the graph). The temperature dependence of the difference, $\Delta\nu$, of the two frequencies is also presented in the upper portion of the graph.

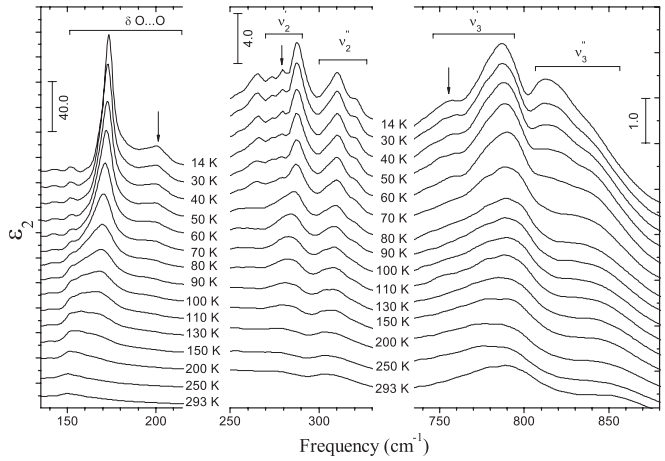

FIG. 7. Temperature dependence of the imaginary part of the dielectric function, $\varepsilon''(\omega,T)$, obtained from IR reflectivity data by Kramers-Krönig inversion: (a) spectral range 140–210 cm^{-1} corresponding to the betaine tetrahedral out-of-plane bending mode; (b) 250–330 cm^{-1}, corresponding to the two nondegenerate ν_2 internal modes of the tetrahedral group; (c) 740–880 cm^{-1}, corresponding to two ν_3 internal modes of the tetrahedral group. The arrows signal the modes whose dielectric strengths are depicted in Fig. 8.

tained from polarized infrared reflectivity data ($\vec{E}\|\vec{b}$), in three selected frequency ranges and at several temperatures between 14 and 293 K. At room temperature and in the spectral range 130–210 cm^{-1} [Fig. 7(a)], we observe a mode located at 152 cm^{-1}. As referred to above, this frequency lies in the range of the out-of-plane bending of the betaine and the tetrahedral groups ($\gamma O\cdots O$ mode).[17–19] This mode is therefore directly related with or strongly coupled to the H bonds between the carboxyl group of betaine and the tetrahedral groups. Consistently with the $x(YY)z$ Raman data, we observe here on cooling the appearance of two additional bands located at about 173 and 200 cm^{-1}. These new bands likely correspond to the activation of the two Raman bands observed in this frequency range (see Fig. 5).

To confirm further this hypothesis, we analyzed the temperature dependence of the dielectric strength of these modes, estimated with the method previously described. Consistently, and as illustrated in Fig. 8(a) with the mode located at about 200 cm^{-1} (at $T=14$ K), the dielectric strength shows a steep decrease as $T\rightarrow T_{c2,b}$.

A similar situation is found in the frequency ranges 250–330 cm^{-1} [Fig. 7(b)] and 740–870 cm^{-1} [Fig. 7(c)], where components of the ν_2 and ν_3 internal modes of the tetrahedral group are located, respectively.[17] Note that the parameters of these modes are expected to reflect directly the ordering of the protons along the quasi-one-dimensional chains formed by the arsenate or phosphate groups. Here, we can detect at room temperature the two components of the ν_2 mode (located near 280 and 305 cm^{-1} at room temperature [see Fig. 7(b)], along with two of the three nondegenerate components of the ν_3 mode (located near 790 and 850 cm^{-1}, Fig. 7(c). On cooling, we observe again the sudden appearance of satellite modes located at about 265 and 322 cm^{-1} [$T=14$ K; Fig. 7(b)] and 750 and 810 cm^{-1} [$T=14$ K; Fig. 7(c)]. As illustrated in Figs. 8(b) and 8(c), the dielectric strength of these satellite modes decreases sharply above $T_{c2,b}$.

These spectroscopic results strongly indicate that the doubling of the unit cell induced by the ordering of the protons along the chains formed by the tetrahedral groups occurs only at $T_{c2,b}$. This result is fully supported by with the fact that typical hysteresis loops are only observed below this critical temperature.

IV. PHASE DIAGRAM

The phase diagram (T, %BP) shown in Fig. 9 summarizes the results presented above for BP25, together with those already published for BP75 and BP52.[12,13] It differs from the hitherto accepted phase diagram, originally proposed in Ref. 7. Although our experimental results agree extremely well with those reported therein whenever the same experimental techniques are used, our use of slightly different methods disclosed new aspects of the phase sequence, which allow us to suggest a somewhat different phase diagram for the mixed system. The main differences are discussed in the following sections.

A. BP75 presents only one phase between 52 and 85 K

As far as it could be experimentally ascertained, BP75 presents a direct paraelectric-antiferroelectric (PE-AFE) phase transition at $T_{c2}\approx 85$ K, which is marked by the appearance of double hysteresis loops and of some new Raman modes. The spike in the dielectric constant observed around 76 K was previously interpreted as another phase transition.[7] Our experimental results, however, reveal that it is a direct consequence of the influence of the internal electric field on the paraelectric-antiferroelectric phase transition.[12]

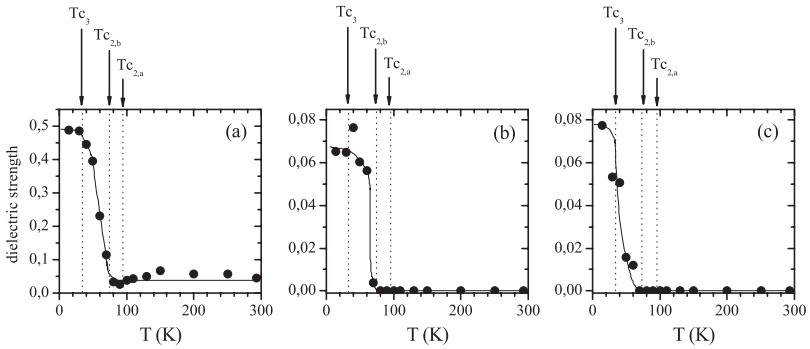

FIG. 8. Temperature dependence of the dielectric strength of the modes located at 200 cm^{-1} (a), 278 cm^{-1} (b), and 756 cm^{-1} (c). These modes are identified in Fig. 7 with arrows.

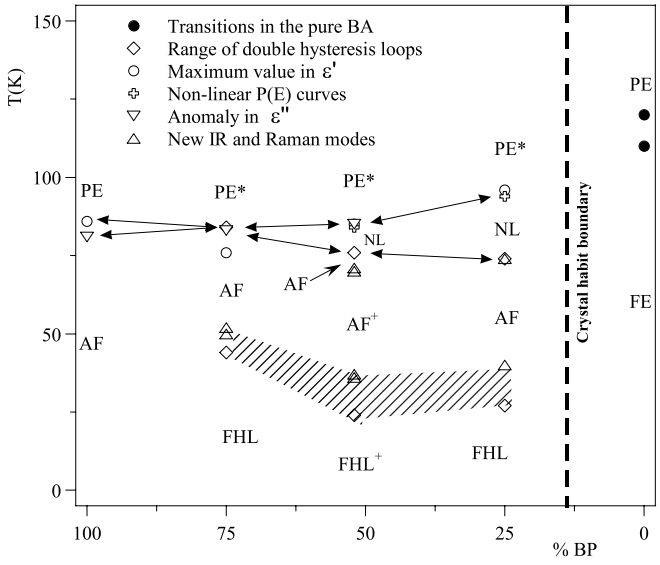

FIG. 9. Phase diagram summarizing the results obtained on the three compositions studied (25%, 52%, and 75% of BP). The following short forms were applied: PE—normal paraelectric phase; PE*—paraelectric phase exhibiting internal field, induced polarization, and linear $P(E)$ curves; NL—phase revealing a nonlinear $P(E)$ curve and internal field; AF (AF+)—ergodic (nonergodic) antiferroelectric phase displaying S-shaped double hysteresis loops and internal electric field; shaded area—intermediate state exhibiting progressive flattening of the double hysteresis loops; FHL (FHL+)—ergodic (nonergodic) phase marked by the absence of double hysteresis loops.

Indeed, the composition with $x=0.75$ seems to be a turning point, as it presents a direct PE-AFE phase transition at T_{c2}. On either side of BP75 in the phase diagram, the single phase transition at T_{c2} apparently splits into two different transitions: to the left, pure BP is known to have one transition at $T'_{c2}=86$ K and another at $T''_{c2}=81$ K. To the right of BP75 in the phase diagram, the single transition at T_{c2} also splits into two distinct transitions, at $T_{c2,a}$ and $T_{c2,b}$, delimiting a temperature interval where the $P(E)$ curves observed are strongly nonlinear: the NL (nonlinear) phase.

B. The intermediate NL phase, observed in BP25 and BP52 between $T_{c2,a}$ and $T_{c2,b}$, is not antiferroelectric

For BP52 and BP25, the maximum of the dielectric constant [maximum slope of the $P(E)$ curve] is observed around $T_{c2,a}\approx 85$ and 96 K, respectively, and is accompanied by the appearance of new Raman lines and the onset of nonlinear $P(E)$ curves (see Fig. 2). The temperature interval between $T_{c2,a}$ and $T_{c2,b}$, is much larger for BP25 than for BP52, as seen in Fig. 9.

It is important to stress that, in both these compounds, double hysteresis loops were never seen in the range $T_{c2,b}<T<T_{c2,a}$. Therefore, the behavior observed in this temperature interval is not antiferroelectric. The transition into the antiferroelectric phase occurs only at $T_{c2,b}\approx 75$ K (BP52) and 74 K (BP25), and is very clearly marked by the onset of double hysteresis loops. $T_{c2,b}$ is also marked in BP52 by the appearance of new IR and Raman lines,[13] and in BP25 by the sharp changes in dielectric strengths of satellite modes [see Figs. 8(a)–8(c)].

C. There is only one low temperature phase for BP75 and BP52

The disappearance of double hysteresis loops at low temperatures is a common characteristic of all the compositions studied.

For BP75, there is a step in $\varepsilon'(T)$ around $T_{c3}\approx 52$ K and an increase in $\Delta\nu(T)$ (see Fig. 6), accompanied by the appearance of new Raman lines. The double hysteresis loops begin to fade down and gradually disappear, over a 5–6 K interval.[12]

For BP52, Raman and IR spectroscopies give clear evidence for structural modifications around the temperature at which the double hysteresis loops begin to fade out. Their gradual vanishing is accompanied by a small maximum of ε'' at $T_{c3}\approx 30$ K.[12]

Lanceros-Méndez *et al.*[7] considered the existence of two different glass phases ($G1$ and $G2$) at low temperatures, for these two compositions. We propose that only one structural low temperature phase occurs. This phase is stabilized over a wide temperature range in which phase coexistence may likely occur. Therefore, the $G1$ phase of Ref. 7 may just correspond to the temperature interval in which the diffuse transformation is in progress (the shadowed area in Fig. 9). We will refer to this low temperature phase as FHL (flattened hysteresis loops) phase.

For BP25, only one low temperature phase ($G1$) was ever proposed.[7] We have also considered a FHL phase for this composition below $T_{c3}\approx 35$ K, where a maximum of ε'' occurs and new Raman lines appear, not least because the behavior of the hysteresis loops below this temperature strongly resembles the low temperature behavior observed in BP52.

V. DISCUSSION AND CONCLUSIONS

Having established the phase diagram presented in the previous section, it still remains to clarify the possible nature of the two unknown phases, the NL and FHL phases that are characterized by nonlinear $P(E)$ curves and by the absence of the double hysteresis loops, respectively. It was previously proposed that the disappearance of the polarization hysteresis loops at low temperatures was related to the onset of a reentrant glass phase;[7] however, our experimental results not only do not support this hypothesis (as mentioned at the end of Sec. III A, no ergodicity breaking was found for either BP25 or BP75),[12] but rather suggest a completely different interpretation. This interpretation will be presented in the discussion that follows.

A. A comparison of $(BP)_x(BA)_{1-x}$ and $(BP)_{1-x}(BPI)_x$

It is worth remembering that the mixed compounds $(BP)_x(BA)_{1-x}$ were generally expected to present glassy behavior at intermediate compositions because of the close

analogy between this mixed system and the well-known mixed system of betaine phosphate and ferroelectric betaine phophite—$(BP)_{1-x}(BPI)_x$,[20–22] which presents such behavior. However, there are also some fundamental differences between the two systems.

First, for $(BP)_x(BA)_{1-x}$, an ordered phase (either antiferroelectric or ferroelectric) is always stabilized at some temperature interval, throughout the whole concentration range.[7,23] Moreover, the mixed compounds $(BP)_x(BA)_{1-x}$ present antiferroelectric behavior to a surprisingly high concentration of the ferroelectric partner, BA. Even BP25, where the ratio of BA to BP is 3 to 1, presents double hysteresis loops in a large temperature interval. This could be related to the extreme stability of the antiferroelectric order in pure BP, which is reflected in the high critical fields (over 4 kV/cm) observed.[2] However, this is in marked contrast with the behavior of the $(BP)_{1-x}(BPI)_x$ system, where certain intermediate concentrations do not present long range order.[24]

Secondly, BP and BPI have very similar chemical formulas, differing only in one oxygen atom, whose place in the tetrahedra is taken up by a hydrogen atom (proton) that appears to have some mobility.[25] In $(BP)_x(BA)_{1-x}$, on the other hand, we have either a P or an As atom in the center of each tetrahedron, which are, therefore, firmly held in their places. In the solid $(BP)_x(BA)_{1-x}$ crystal, each site of the lattice contains either BA or BP, and these cannot be swapped or interchanged without a significant change of the crystal structure. Therefore, in a $(BP)_x(BA)_{1-x}$ crystal the possible configurations have to obey much more serious constraints than in $(BP)_{1-x}(BPI)_x$.

B. Some important characteristics of the $(BP)_x(BA)_{1-x}$ mixed solutions

Another interesting feature of the $(BP)_x(BA)_{1-x}$ system is that triple hysteresis loops are never observed. For the three compositions studied (BP75, BP52, and BP25), the antiferroelectric behavior observed between $T_{c2,b}$ and T_{c3} clearly does not coexist with any form of ferroelectric or ferrielectric response. Apparently, large ferroelectric domains of BA origin do not form in these solid solutions. The antiferroelectric behavior seems to result from a ferroelectric ordering within each one-dimensional chain (which is natural to both BA and BP),[7] combined with an antiferroelectric ordering of nearby chains that can be induced by an amount of BP as small as 25%.

The chains themselves would then contain a large number of defects of several possible types,[26] for example

⋯-BA-BP-BA-BA-BP-BA-BP-BP-BA-BP-BA-BP-BP-BP

-⋯

⋯-BA-BA-BA-BP-BA-BP-BP-BA-BA-BP-BA-BA-BP

-BA-⋯

Some of these defects may have an intrinsic dipole moment, and the combined effect of such dipole moments is one possible explanation for the internal electric fields observed. These internal fields are revealed by pyroelectric measurements, are present even in the paraelectric phase and become increasingly stronger as the content of BA in the sample increases [see Figs. 2 and 3(d)].

The sublattice polarization in the antiferroelectric phase seen as a function of temperature and composition [Fig. 3(a)], points to another interesting aspect, as the sublattice polarization of BP75 is less than half that of pure BP ($\sim 4 \times 10^{-3}$ C/m^2), but not much higher than that of BP52.

This reduced value of the saturated sublattice polarization in BP75, combined with the absence of a ferroelectric or ferrielectric response, suggest some form of partial cancellation of the polarization within the chains. This seems to result not only from the competing FE and AFE interchain interactions but also from the need to maintain ferroelectric order within each chain. Since the BA parts of the chain favor a dipolar moment parallel to the neighboring chains while the BP parts of the chain favor the opposite, there will be a spatial inhomogeneity of competing ferroelectric and antiferroelectric interactions. The compromise solution could likely be a reduced dipole moment along the chain, leading in turn to a smaller sublattice polarization in the antiferroelectric phase.

This hypothesis gives a good explanation for the low value of the sublattice polarization in BP75, but the similar values of the sublattice polarization in BP75 and BP52 are still puzzling. In fact, the introduction of only 25% of BA lowers the sublattice polarization to half of its value in the pure compound, but nearly twice that amount of BA does not do much more (see Figure 2(a)). We suggest that in BP52 (and possibly also in BP25), the spatial inhomogeneity of competing ferroelectric and antiferroelectric interactions, together with the rigid constraint which keeps the P and As atoms in their original positions in the chain, could lead to a compromise solution such as an "imperfect antiferroelectric order," where dipoles in neighboring chains are antiparallel but the dipole moments along the chain are not uniform due to a disordered polar cluster arrangement. An exaggerated example of a nonuniform dipole moment configuration is depicted schematically below:

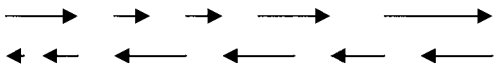

(1)

This structure would still present a macroscopic antiferroelectric behavior, yet it is also characterized by a certain spatial disorder, as the polarization is not spatially uniform and the strength of the individual dipole moments may depend somewhat on the past history of the sample (cooling rate, applied fields, etc.). A nonergodic behavior still well within the range of the antiferroelectric phase would be expected, as it is observed in BP52 from pyroelectric data.[13]

This imperfect antiferroelectric order probably also occurs in the case of BP25. However for BP75, the value of the sublattice polarization suggests that the preferred mechanism is a strong uniform reduction of the dipole moments along the chain. This may be due to the incompatibility between the imperfect antiferroelectric order and the geometrical configuration of the betaine molecules, since the Raman data indicate that this compound is strongly BP-like in its geometrical configuration. The rigidity of the BP structure

makes a compromise solution of nonuniform dipoles more difficult and favors a uniform reduction of the dipole moments along the chain.

C. The NL (nonlinear) phase

The structure stabilized between $T_{c2,a}$ and $T_{c2,b}$ is characterized by nonlinear $P(E)$ curves. At $T_{c2,a}$ the dielectric constant presents the highest value in the temperature range studied, disclosing a structure with high polarizability. The additional bands identified by Raman spectroscopy show clearly that some breaking of symmetry occurs, at least on a mesoscopic scale.

The sum of these results and the fact that they are much more relevant in BP25, clearly reflect that the nonlinear behavior is driven by the BA partner. It is possible that the interactions between BA molecules disseminated in a matrix of BP could be attenuated by these BP molecules: consequently, polar clusterlike states can be formed exhibiting strong polar short range interactions but devoid of long ferroelectric interactions due to the presence of BP. Thus, the NL phase presents very prominent polar properties, in some ways resembling those of a superparaelectric. Moreover, the temperature stability range of the NL phase increases with increasing content of BA (Fig. 9). On the one hand, $T_{c2,a}$ increases with increasing BA content, but takes values always lower than 120 K which corresponds to the transition temperature to the ferroelectric phase in betaine arsenate. On the other hand, $T_{c2,b}$ decreases with increasing BA content, thus approaching the temperature where the ordered antiferroelectric arrangement imposed by BP is attained.

D. The low temperature FHL (flattened hysteresis loops) phase

The nature of the FHL phase is still not completely understood. The transition from the antiferroelectric phase to the FHL phase is not accompanied by a sudden disappearance of double hysteresis loops but rather by a progressive flattening of these loops, as if originating from the loss of some degrees of freedom. In this case, a low temperature disordered phase would be expected. However, the study of thermal cycles did not disclose in BP75 and BP25 any evidence of nonergodicity in the FHL phase, and, in the case of BP52, only a moderate nonergodic response was observed well within the antiferroelectric phase. It is also puzzling that BP75 has the highest T_{c3} and consequently the largest interval of stability of the FHL phase, because this compound seems to be the most ordered composition among all those we have studied: the $P(E)$ curves shown in Fig. 2(c) are only slightly deformed and present a clear separation of the Raman lines around 2997 cm^{-1} at low temperatures, which is considered a typical feature of a BP-like structure.

The spatial inhomogeneities in competing ferroelectric and antiferroelectric interactions, combined with the need for ferroelectric ordering within each chain and the rigid constraints arising from the unchangeable localizations of phosphorus and arsenic atoms inside the tetrahedral groups, give rise to a nonuniform distribution of dipole moments which, in turn, causes an internal electric field along the chain that increases with increasing arsenate content. The presence of this internal field can impose extra ordering in the system as the temperature is lowered, avoiding in this way some kind of disorder due to the loss of several degrees of freedom. The BP-like geometrical configuration, evidenced by all compositions studied, would also favor a more ordered structure in the lower temperature range. This ordering process could well justify the gradual decrease of the sublattice polarization P_{sub} that occurs below T_{c3}.

ACKNOWLEDGMENTS

This work was supported by "Programa FEDER/POCTI (Projecto No. 2-155/94 da Fundação para a Ciência e a Tecnologia)" and "Projecto No. POCTI/FIS/14287/2001 da Fundação para a Ciência e a Tecnologia."

*Email address: amalmeid@fc.up.pt

[1] A. Klöpperpieper, H. J. Rother, J. Albers, and K. H. Ehses, Ferroelectr., Lett. Sect. **44**, 115 (1982).
[2] J. Albers, A. Klöpperpieper, H. J. Rother, and K. H. Ehses, Phys. Status Solidi A **74**, 553 (1982).
[3] W. Schildkamp and J. Spilker, Z. Kristallogr. **168**, 159 (1984).
[4] W. Schildkamp, G. Schäfer, and J. Spilker, Z. Kristallogr. **168**, 187 (1984).
[5] J. Albers, Ferroelectrics **78**, 3 (1988).
[6] S. Hayase, T. Koshiba, H. Terauchi, M. Maeda, and I. Suzuki, Ferroelectrics **96**, 221 (1989).
[7] S. Lanceros-Méndez, H. Ebert, G. Schaack, and A. Klöpperpieper, Phys. Rev. B **67**, 014109 (2003).
[8] O. Freitag, H. J. Brüchner, and H.-G. Unruh, Z. Phys. B: Condens. Matter **61**, 75 (1985).
[9] A. Bussmann-Holder and H. Bilz, Ferroelectrics **54**, 5 (1984).
[10] U. T. Höchli, K. Knorr, and A. Loidl, Adv. Phys. **39**, 405 (1990).
[11] M. Manger, S. Lanceros-Méndez, G. Schaack, and A. Klöpperpieper, J. Phys.: Condens. Matter **8**, 4617 (1996).
[12] A. Almeida, S. Sarmento, J. L. Ribeiro, L. G. Vieira, M. R. Chaves, and A. Klöpperpieper, Ferroelectrics **295**, 9 (2003).
[13] A. Almeida, S. Sarmento, J. L. Ribeiro, L. G. Vieira, M. R. Chaves, and A. Klöpperpieper, Integr. Ferroelectr. **63**, 143 (2004).
[14] Maeda, Ferroelectrics **96**, 529 (1989).
[15] R. Chaves, H. Amaral, and S. Ziolkiewicz, J. Phys. (Paris) **41**, 259 (1980).
[16] M. M. Ilczyzyn and H. Ratajczak, J. Mol. Struct. **375**, 213 (1996).
[17] *Handbook of Chemistry and Physics*, 70th ed. (Chemical Ruben Company, Boca Raton, FL, 1989).
[18] A. Novak, *Structure and Bonding* (Springer-Verlag, Berlin-Heidelberg, 1974), Vol. 18, p. 177.
[19] Z. Ouafik, N. le Calvé, and B. Pasquier, Chem. Phys. **194**, 145

(1995).
[20] M. L. Santos, J. C. Azevedo, A. Almeida, M. R. Chaves, A. R. Pires, H. E. Müser, and A. Klöpperpieper, Ferroelectrics **108**, 363 (1990).
[21] S. L. Hutton, I. Fehst, R. Bohmer, M. Braune, B. Mertz, P. Lunkenheimer, and A. Loidl, Phys. Rev. Lett. **66**, 1990 (1991).
[22] J. Banys, C. Klimm, G. Völkel, H. Bauch, and A. Klöpperpieper, Phys. Rev. B **50**, 16751 (1994).
[23] M. Maeda and I. Suzuki, Ferroelectrics **108**, 351 (1990).
[24] M. L. Santos, M. R. Chaves, A. Almeida, A. Klöpperpieper, H. E. Müser, and J. Albers, Ferroelectr., Lett. Sect. **15**, 17 (1993).
[25] M. L. Santos, L. C. R. Andrade, M. M. R. Costa, M. R. Chaves, A. Almeida, A. Klöpperpieper, and J. Albers, Phys. Status Solidi B **199**, 351 (1997).
[26] H. Bauch, G. Völkel, R. Böttcher, A. Pöppl, H. Schäfer, J. Banys, and A. Klöpperpieper, Phys. Rev. B **54**, 9162 (1996).